J Mater Sci: Mater Med (2008) 19:583–589
DOI 10.1007/s10856-007-3194-3

Protein incorporation within Ti scaffold for bone ingrowth using Sol-gel SiO_2 as a slow release carrier

Tal Reiner · Shifra Kababya · Irena Gotman

Received: 5 December 2006 / Accepted: 22 May 2007 / Published online: 10 July 2007

Abstract Porous titanium structures hold considerable promise as scaffolds for bone ingrowth in load bearing locations provided they are made osteoinductive by incorporation of bone growth factors. The purpose of the present research was to incorporate soybean trypsin inhibitor (STI) imitating growth factor into a porous Ti scaffold using sol-gel silica as a slow-release protein carrier. Alcohol-free TMOS-based sols (of pH 2 or 5) with dissolved STI were injected into Ti wire scaffolds yielding SiO_2 coating on the wire struts and SiO_2 beads entrapped in-between the wires. The formation of well-polymerized nanoporous SiO_2 was confirmed by FTIR, solid-state NMR, N_2 adsorption/desorption isotherms and BET analysis. In-vitro dissolution of silica and STI release in phosphate buffered saline (PBS) at 37 °C were measured by ICP-AES and Bradford assay, respectively. The biochemical activity of released STI protein was assessed by enzymatic assay. STI release was found to follow an attractive pattern of rapid release during the first 5 days followed by steady slow release for over one month. Despite certain conformational changes induced by the encapsulation procedure (detected by Circular Dichroism), the released STI retained most of its biological activity, especially when silica sol was prepared at the high protein-friendly pH = 5.

T. Reiner · I. Gotman (✉)
Faculty of Materials Engineering, Technion-IIT, Haifa 32000, Israel
e-mail: gotman@tx.technion.ac.il

S. Kababya
Schulich Faculty of Chemistry, Technion-IIT, Haifa 32000, Israel

Introduction

Many medical situations call for bone grafts in order to repair fractures or assist skeletal reconstruction after bone loss secondary to trauma, infection or tumor removal. Autogenous cancellous bone is considered the ideal bone graft material, however it is not available in sufficient amounts and its harvesting imposes health concerns such as infections, blood loss and donor site instability. Allograft bone, though available in considerable amounts, does not have the osteogenic potential of the autogenous bone and has the disadvantage of eliciting an immunological response and the risk of inducing transmissible diseases. Consequently considerable attention has been directed towards the development of synthetic bone replacement materials. The currently used bone graft substitutes (mainly porous hydroxyapatite or other Ca phosphate ceramics) are osteoconductive and can be eventually incorporated in the surrounding bone, however none of them is sufficiently strong to stand in as a complete replacement for load-bearing bones [1, 2]. Porous metal structures, on the other hand, can act as strong scaffolds for bone ingrowth. Of all surgical metals, titanium seems most promising as it allows direct apposition of the bone tissue [3]. Ti alloys also have the advantage of a relatively, low elastic modulus which minimizes the stress-shielding phenomenon [4]. Used on their own, however, porous Ti scaffolds will be unable to mend large bone defects due to their lack of osteoinductivity. Osteoinductivity is the ability of the implant to induce stem cells or osteoprogenitor cells to differentiate into osteoblasts. This property has been attributed to bone morphogenetic proteins (BMP), mostly cytokines of the TGF-β (transforming growth factor-β) super-family, which are associated with the collagen component of bone [5]. For clinical benefit, these growth factors must be delivered directly to the site of regeneration via a carrier matrix and administered via a controlled delivery system [6]. This can be achieved if a porous Ti scaffold is made a carrier for BMP delivery, e.g. by coating with a tissue-friendly layer capable of slowly releasing BMP into the body fluids. One solution is the incorporation of BMP in the three-dimensional inorganic latticework of biomimetic Ca-P coatings by co-precipitation at the time of their deposition. Thus incorporated BMP-2 has been shown to retain its potency to stimulate the osteogenic activity of cultured osteoprogenitor cells in vitro and to induce bone formation at an ectopic site in vivo [7, 8].

Alternatively, sol-gel processed silica glasses have been studied as controlled release matrices. These materials are resorbable, highly porous and nanostructured [9]. Sol-gel silica glass dissolution occurs via a hydrolysis reaction: $SiO_{2(s)} + 2H_2O \rightarrow Si(OH)_{4(aq)}$ [10]. The dissolution products of silica and bioglasses are non-toxic at low concentrations and have even been found to be stimulatory to bone-forming cells [11, 12]. Room-temperature sol-gel processes have been developed that allow the addition and uniform distribution of biological agents in the liquid sol. After gelation, condensation and drying, the agents become encapsulated in a glassy solid. Modifying the conventional sol-gel procedures towards alcohol-free and mild pH conditions should favor the retention of the native conformation and biochemical activity of proteins. The potential of sol-gel derived silica glass matrices for incorporation and sustained release of antibiotic drugs, TGF-β1 growth factor and of albumin (BSA) and Soybean trypsin inhibitor (STI) proteins have been demonstrated in vitro [13–16]. Nevertheless, coating metallic bone-ingrowth scaffolds with silica glass layers capable of slowly releasing proteins or drugs into the body fluids has not been reported. Therefore, the main thrust of the present work was to study the incorporation of biologically active protein within porous Ti structures using sol-gel silica as a slow-release protein carrier.

Materials and methods

Materials and scaffolds

Soybean Trypsin inhibitor (STI) was used as the model protein for bone growth factor. STI was chosen because its size (21 kDa) is comparable to those of the TGF-β1 (25 kDa) and BMP-2 (26 kDa) growth factors, and its in vitro release kinetics from biodegradable carriers is reportedly similar to that of BMPs [17].

STI, as well as Tetramethyl-orthosilicate (TMOS), HCl, Sodium phosphate buffer (pH = 7) and PBS (phosphate buffered saline, pH = 7.4) were purchased from Sigma Chemical Co.

Ti wires (0.2 mm diameter) and Ti wire mesh, having volumetric porosity of 40%, density of 1.8 g/cm^3, fiber diameter of 0.3 mm and average distance between fibers of 0.5 mm, were purchased from Performance Materials and Alloys Ltd. (NJ, U.S.A.). The mesh was coiled and pressed in a rigid die at 60 MPa to produce prototype porous scaffolds. The obtained scaffolds were cylindrical 3D wire structures 6 mm in diameter and 15 mm high, (Fig. 1), with the yield stress (σ_y) of 45 MPa.

Before being coated with sol-gel glass, part of the 3D scaffolds and separate Ti wires were soaked in 5M NaOH at 60 °C for 24 h [18].

Silica synthesis

Sol-gel silica coatings were prepared by hydrolysis and polycondensation of tetramethyl orthosilane (TMOS ≥ 98%, Fluka) according to a procedure suggested by Radin et al. [14] for bulk silica glass. In order to prevent denaturation of encapsulated STI, no alcohol was used in TMOS hydrolysis and the synthesis was conducted at room temperature. It has been reported that when similar size proteins were encapsulated in silica, synthesized from the same precursors, their structure remained relatively unaltered [19].

5 mL TMOS were added to 5.4 mL water while magnetically stirring and stirred for additional 5 min. 0.1 mL of 1 M HCl or 1 mM HCl were added and stirred for 30 min and 1 h, respectively. 0.9 mL of the obtained silica sol was mixed with 0.1 mL of buffer solution (pH = 7) that contained 10 mg STI, and sonicated. The protein was added as a solution in order to ensure its homogeneous distribution. The final pH was 2 and 5.1 for the sols prepared using the 1 M and 1 mM HCl, respectively. Increasing the pH shortens the gelation time which affects the sol-gel handling characteristics.

To obtain silica coating, Ti wires were dipped in and 3D wire structures were injected with the sol and let dry in a container at room temperature for 2 days. The wires and 3D scaffolds were weighed before and after coating to assess the silica coating thickness. In addition, silica granules (with and without entrapped STI) were prepared

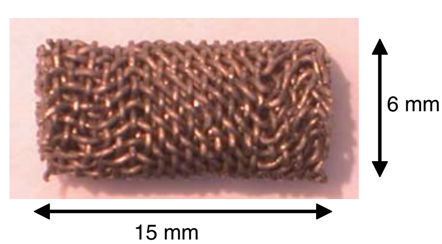

Fig. 1 A prototype Ti wire scaffold

by letting the sol gelate for 1 day, cutting the gel into small pieces (< 1 mm) and drying at room temperature. To estimate the density of the obtained silica, 3 mm diameter by 10 mm height cylinders were prepared by pouring the sol into a plastic mold.

In vitro test

In-vitro dissolution behavior and STI release of sol-gel treated Ti was studied in phosphate buffered saline, PBS (pH = 7.4). Three 3 cm long wires or one wire cylinder were placed into 20 mL PBS and kept at 37 ± 0.5 °C for four weeks. The temperature was maintained using a water bath. The solution was replaced after specific intervals ranging from 1 h (in the beginning of the experiment) to 1 week (towards the end of the experiment), and tested for Si ion and STI contents.

Si concentration in the solution was measured by, Inductively Coupled Plasma combined with Atomic Emission Spectroscopy, ICP-AES (Varian, Vista AX). Protein content (values in the order of μg/mL) was assessed by Bradford assay. Bradford assays were preformed using Varian (Cary 100 scan) spectrophotometer.

Silica characterization

Sol-gel silica coated Ti wires and 3D structures before and after dissolution tests were investigated in a high resolution SEM (HRSEM) LEO 982. Silica before and after dissolution tests was characterized by FTIR spectroscopy (Bruker Equinox 55, transmittance mode) using the conventional KBr pellet methodology.

Specific surface area, pore volume and average pore size of sol-gel silica granules before and after immersion were measured by the Brunauer-Emmett-Teller method (BET) and by the analysis of nitrogen adsorption and desorption isotherms (Quantachrome Nova e-3000).

SiO_2 granules were also characterized by ^{29}Si solid state MAS NMR. The experiments were carried out on a 300-MHz Chemagnetics/Varian CMX-*Infinity* using a Chemagnetics double resonance MAS probe with high performance zirconia rotors (7.5 mm o.d.), at 59.606 MHz, and spinning rate of 5000 Hz. ^{29}Si MAS NMR spectra were obtained by direct excitation combined with spin echo and high power proton decoupling of 100 kHz. Pulse widths of 5 and 10 μs were employed for the $\pi/2$ and π pulses, respectively, and 200 μs echo interval. To maintain the peak areas quantitative repetition delays of 600 s were used. 64 to 100 signal accumulations were collected to obtain adequate signal-to-noise (S/N). Sample weights were 150–300 mg. The chemical shift scale was referenced to TMS.

Assessment of protein activity

0.2 g of the sol-gel silica granules with encapsulated STI were immersed in 10 mL PBS at 37 °C for 6 days. Protein content in solution was assessed by absorption intensity at 275 nm using absorption extinction coefficient,

$$\lambda_{275nm} = 0.8226 \frac{mL}{mg \cdot cm},$$

found by calibration.

The biochemical activity of STI protein released from silica granules after 6 days immersion was assessed by enzymatic assay. First, trypsin activity was measured spectrophotometrically at 253 nm (Varian, Cary 100 scan) using the synthetic substrate benzoyl arginine ethyl ester (BAEE) in 50 mM phosphate buffer, pH 7.6, at 25 °C. Then, trypsin inhibitory activity of STI was determined by measuring the reduction of trypsin-catalyzed hydrolysis of BAEE.

The effect of encapsulation procedure on STI protein structure was assessed by UV absorption (Varian, Cary 100 scan) and Circular Dichroism (CD) spectroscopy. CD spectra were taken on a JASCO J-500C spectropolarimeter. Protein concentration was 0.3 mg/mL and 33 μg/mL for "near UV" and "far UV" CD analyses, respectively.

Results and discussion

The alkali treatment of Ti wires and 3D scaffolds resulted in the formation of a nano-porous network surface layer, (Fig. 2), morphologically resembling the surface of likewise treated flat Ti coupons originally reported in ref. 18. AES depth profiling detected significant amounts of Na and O (in addition to Ti) near the surface of the alkali-treated Ti wire suggesting a sodium titanate hydrogel layer similar to the one formed on alkali-treated flat Ti surfaces [18]. As will be shown below, this surface morphology improved the adhesion of the sol-gel silica coating.

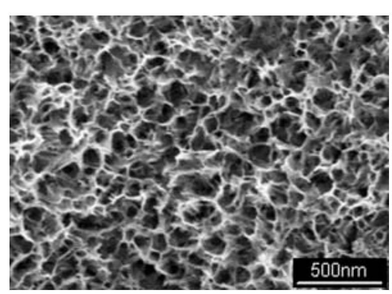

Fig. 2 SEM micrograph of alkali treated Ti wire

Dipping Ti wires in the sol (pH = 2) followed by 2 days drying produced a relatively uniform silica coating, (Fig. 3a). Following sonication, the coating remained tightly bound to the alkali treated wires. This is in contrast to the coating on untreated wires that spalled off the metal surface during sonication.

Based on the weight gain and on the measured sol-gel silica density (1.4 g/cm^3), the average coating thickness was 1.8 μm. This compares quite well with the coating thickness of 1.5 to 2.5 μm measured along the wire length in SEM, (Fig. 3c). A high magnification SEM image, (Fig. 3b), shows that the coating is nanoporous with pore size ≤ 5 nm.

When immersed in PBS at 37 °C, the coating underwent rapid dissolution during the first 24 h, followed by very slow dissolution over the period of several days, (Fig. 4). After 5 days in PBS, the remaining silica layer was extremely thin and the underlying nanoporous Ti surface was exposed to view in SEM, (Fig. 5).

A 3D wire structure, shown in Fig. 1, was injected with silica sol (pH = 2) and dried. Polymerization of the sol yielded silica coating on the wire struts and also silica beads trapped in-between the wires. Weight gain following injection/drying was 64 mg, of which ~ 7 mg (11%) was the coating (assuming 2 μm thickness) and the rest (89%) were the beads. The total protein load was 2.7 mg, silica beads being the main STI carrier.

FTIR spectrum of silica beads removed from the wire structure (not shown) was typical of well-polymerized silica, indicated by strong and sharp Si-O-Si bands at 465, 800, 1088 and 1246 cm^{-1}. The absence of C-H bands over 2800–3000 cm^{-1} suggested complete hydrolization of the methoxy groups during the sol-gel synthesis.

To better understand the structure of silica beads formed within the wire structure, separately prepared silica granules were examined in BET and NMR. The results of BET-N_2 adsorption/desorption analysis, Table 1, show that the synthesized silica is very porous (~45% porosity, based on the pore volume), the average pore size being 2.3 nm.

NMR ^{29}Si chemical shift echo spectra of silica granules, Fig. 6, exhibit Q^2 ($Si(OSi)_2(OH)_2$) peak at –91.1 ppm, Q^3 ($Si(OSi)_3(OH)_1$) peak at –100.7 ppm and Q^4 ($Si(OSi)_4$) peak at –111.0 ppm [20]. No TMOS reagent peaks are detected indicating its complete conversion. The spectra of as-synthesized silica with and without STI protein are practically identical, (Fig. 6) and (Table 2), suggesting that protein presence and encapsulation doesn't affect the resulting silica network structure.

Figure 7 shows the kinetics of silica dissolution and STI release from the wire structure into PBS. We assume that the initial rapid dissolution of silica (first several days) is the superposition of the coating and beads dissolution. Based on the dissolution behavior of separate sol-gel treated wires (Figs. 4 and 5), it may be assumed that after 5–6 days immersion the coating on the struts of the 3D wire structure has been fully dissolved and only the silica beads continue to dissolve and release STI. After 4 weeks in PBS, the beads still retain their initial shape, however their surface is eaten away by dissolution and becomes more irregular than before immersion.

The intensities of the Q^2 and Q^3 NMR peaks associated with the silanol (Si-OH) surface groups decrease after 2 weeks immersion relative to the intensity of the Q^4 peak of bulk silicon, (Fig. 6). Similarly, the bands corresponding to surface silanol in FTIR spectra of the silica granules (not shown) become weaker after 4 weeks immersion. It should

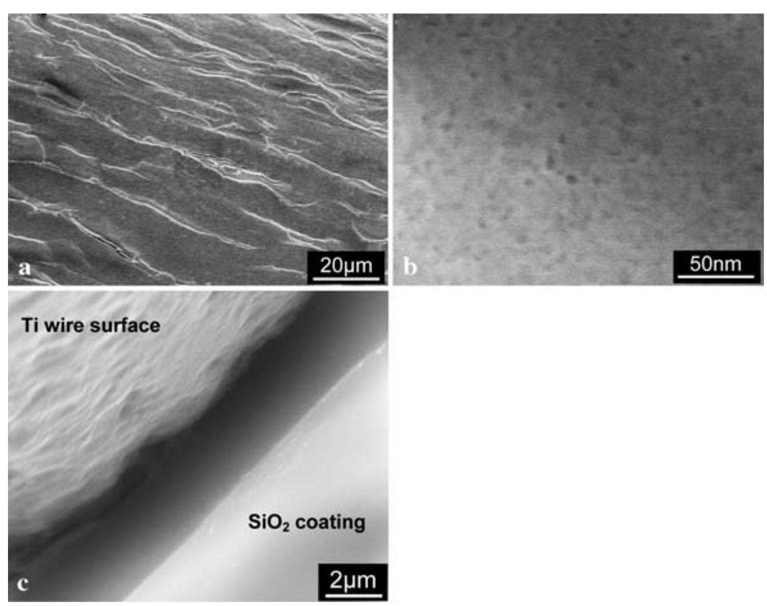

Fig. 3 SEM micrographs of as-synthesized sol-gel silica + STI coating on Ti wire: **a,b**–top view; **c** - cross-section

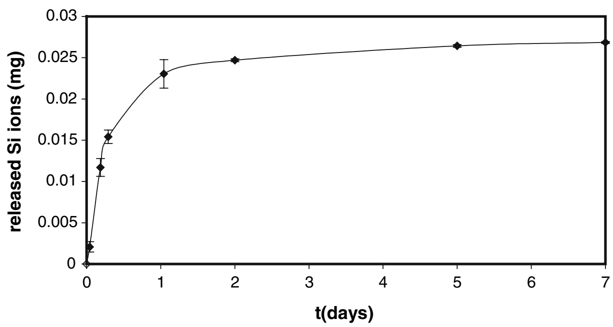

Fig. 4 Cumulative release of Si to PBS from silica + STI-coated wires as a function of immersion time

Table 1 Characteristics of silica granules with encapsulated STI obtained from the results of BET test and N_2 adsorption-desorption isotherms

	As prepared	After 4 weeks in PBS
Specific surface area (m^2/g)	585.2	338.4
Total pore volume (cm^3/g)	0.3351	1.2
Average pore diameter (nm)	2.291	14.18

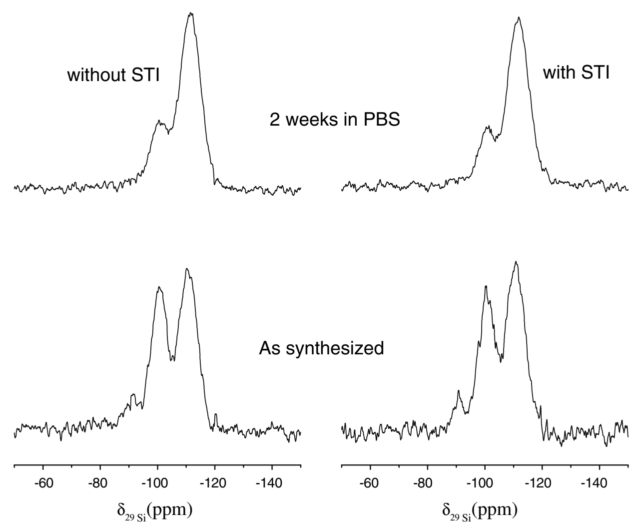

Fig. 6 59.6 MHz ^{29}Si NMR chemical shift echo spectra of silica with and without encapsulated STI; as-synthesized and after 2 weeks immersion in PBS

also be noted that more effective dissolution occurs when protein is present, as implied by the 4% increase of Q^4 compared to samples without protein present (Table 2). These observations are in agreement with an approximately 2-fold specific surface area decrease measured by BET after 4 weeks immersion, Table 1. In addition, the BET-N_2 adsorption/desorption analysis has shown an increase in the total pore volume and significant pore coarsening (from 2.3 to 14.2 nm). Similar changes in the surface area and pore size during immersion of sol-gel silica in buffer solution were reported by Santos et al [14], suggesting that silica dissolution occurs via the coarsening and coalescence of initial nanopores.

STI release into PBS roughly follows the silica dissolution pattern,(Fig. 7). Rapid STI release is observed at the initial immersion stages with ~50% STI released during the first 5 days. This is followed by a 'steady-state' release from the silica beads. By the end of one month, ~80% STI has been released whereas only ~25% of silica has dissolved over the same period. This suggests that silica dissolution is not the only mechanism of STI release. Another mechanism of STI release may be out-diffusion of the protein.

The results of enzymatic assay - trypsin activity as a function of added STI amount–are shown in Fig. 8. The inhibiting activity of STI released from silica prepared at pH 2 was somewhat lower than that of the unprocessed protein as indicated by the more moderate graph slope. The same effect was observed for fresh STI dissolved in aqueous solution of pH 2. When the pH of the silica sol was increased to 5, practically no loss of activity of the encapsulated STI was observed. Similarly, the activity of fresh STI was unaffected by dissolution in aqueous solution of pH 5. This suggests that the biochemical activity of encapsulated STI is affected by the silica sol acidity. The result is not unexpected since large pH deviations from the optimal value (pH = 7) have been reported to disturb hydrogen bonds holding the reactive loop of STI in the favorable conformation [21].

In order to test the effect of sol-gel encapsulation on STI protein structure, UV and CD analyses were performed. UV spectra of STI released from silica granules prepared at

Fig. 5 SEM micrographs of sol-gel silica + STI coating on Ti wire after 5 days immersion in PBS

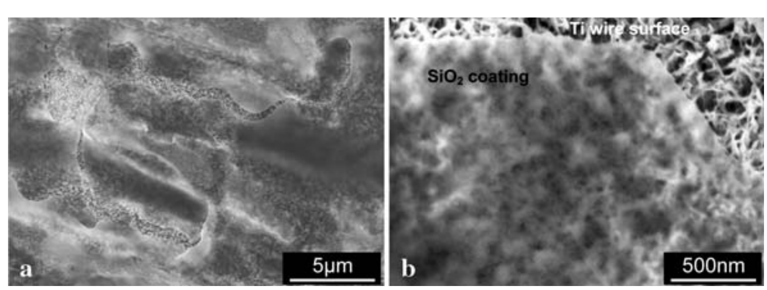

Table 2 Relative abundances (%) of the Q^2, Q^3, Q^4 forms in silica beads synthesized with and without STI protein, and after 2 weeks immersion in PBS

	Q^2	Q^3	Q^4
δ (ppm)	91.1	101.0	111.0
Without STI	7.7	42.5	49.8
With STI	7.1	40.9	52
Without STI after 2 weeks	3.2	25.2	71.6
With STI after 2 weeks	2.3	21.9	75.8

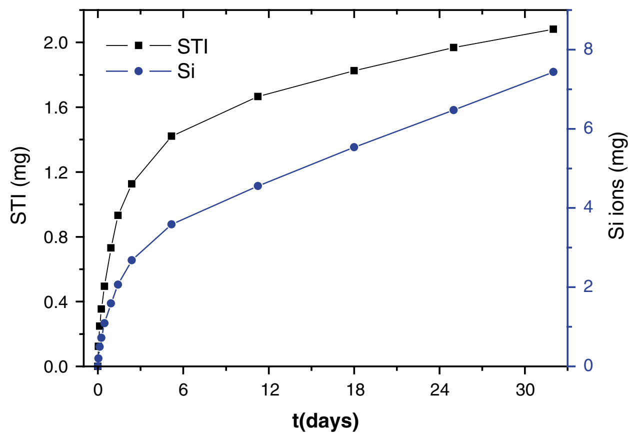

Fig. 7 Cumulative Si (blue line) and STI (black line) release to PBS from the injected Ti wire structure as a function of immersion time

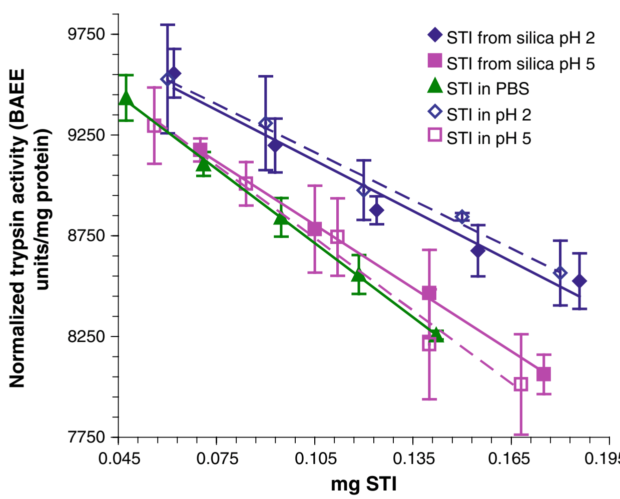

Fig. 8 Trypsin activity as a function of the added amount of STI (enzymatic assay): STI released in PBS after 6 days immersion from silica synthesized at pH 2 (blue solid line) and at pH 5 (pink solid line); unprocessed STI dissolved for 6 days in PBS (green line) and in aqueous solutions of pH 2 (broken blue line) and pH 5 (broken pink line)

pH 2 and 5 are similar to that of unprocessed STI (Fig. 9). This suggests that no denaturation of STI occurred in the course of sol-gel encapsulation at either pH.

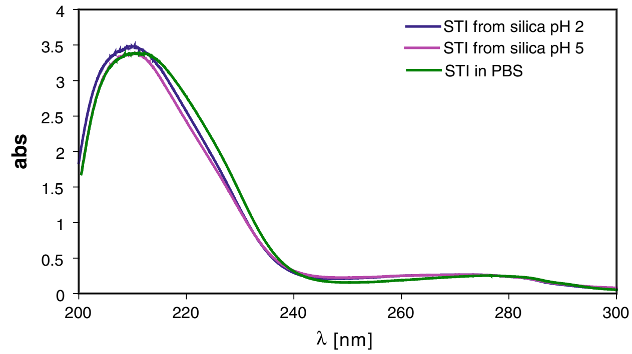

Fig. 9 UV spectra of STI released in PBS after 6 days immersion from silica synthesized at pH 2 (blue line) and at pH 5 (pink line) and of unprocessed STI dissolved for 6 days in PBS (green line)

CD spectra of STI released from the silica granules prepared at pH 2 and 5 are also similar, however they are noticeably different from the spectra of the unprocessed protein, (Fig. 10). Differences are observed both in the near UV (240–350 nm) and far UV (200–240 nm) regions suggesting that sol-gel encapsulation affects both the overall tertiary structure and the secondary structure elements (alpha-helix, beta-sheet, random coils) of STI.

Based on the results of enzymatic assay, (Fig. 8), the detected conformational changes don't impair STI activity, suggesting that the short reactive loop of STI consisting of only seven amino acid residues [21] is unaffected by the encapsulation procedure.

The effect of low pH on the biochemical activity of the released and unprocessed STI (Fig. 8), doesn't show up in any change of the corresponding CD spectra (Fig. 10). This, again, could be due to the short length of the active loop, the conformational alterations being too small (though sufficient to affect STI activity) to be detected by CD spectroscopy.

It is worth noting that STI protein was used in this research only as a model for a growth factor. Growth factors

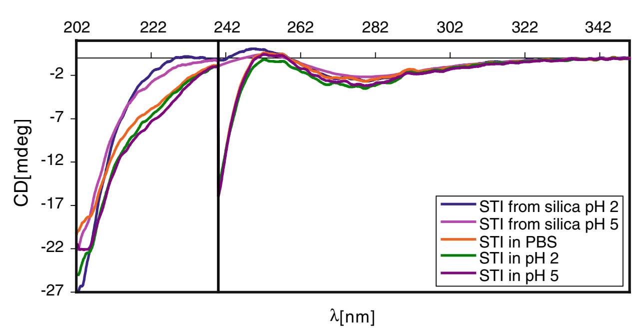

Fig. 10 CD spectra of STI released in PBS after 6 days immersion from silica synthesized at pH 2 (blue line) and at pH 5 (pink line), and of unprocessed STI dissolved for 6 days in PBS (orange line) and in aqueous solutions of pH 2 (green line) and pH 5 (purple line)

are typically less stable and exert more sophisticated biological effects. Our observation that the biochemical activity of the STI protein was not affected by encapsulation procedure cannot be applied directly to growth factors. Similarly to STI, the conformation of a growth factor can be changed by encapsulation, and this, in turn, may damage the protein activity.

Conclusions

A biochemically active STI protein modeling bone growth factor was incorporated within porous Ti scaffolds intended for bone-ingrowth using sol-gel silica as a slow-release protein carrier. The injection of protein-containing sol into the porous scaffold produced a hierarchical silica structure consisting of a ~ 2 μm thick coating on the wire struts and silica beads ~ 0.5 mm in size trapped in-between the wires. The synthesized silica was ~ 45% porous with an average pore size of 2.3 nm. Immersion in PBS resulted in silica dissolution and STI release following an attractive pattern of rapid release during the first 5 days followed by steady slow release for over one month. According to the FTIR, solid state NMR and BET analyses, silica dissolution occurred via the coarsening and coalescence of initial nanopores. STI was released together with silica dissolution as well as by out-diffusion. Despite certain conformational changes induced by the encapsulation procedure, the released STI retained most of its biological activity, especially when the silica sol was prepared at the protein-friendly pH of 5. Applying the reported encapsulation procedure to a real bone growth factor will allow us to produce strong osteoinductive bone graft substitutes for load-bearing locations provided the growth factor retains its ability to induce cell differentiation.

Acknowledgments This work was supported by Israel Science Foundation–ISF through research grant No. 1193/05. The authors are grateful to Prof. E.Y. Gutmanas, Faculty of Materials Engineering, Technion, and Prof. A. Schmidt, Schulich Faculty of Chemistry, Technion, for their assistance and helpful comments.

References

1. J. W. M. VEHOF, P. H. M. SPAUWEN and J. A. JANSEN, *Biomaterials* **21** (2000) 2003
2. D. C. METSGER, M. R. RIEGER and D. W. FOREMAN, *J. Mater. Sci.: Mater. Med.* **10** (1999) 9
3. J. C. KELLER, C. M. STANFORD, J. P. WIGHTMAN, R. A. DRAUGHN and R. ZAHARIAS, *J. Biomed. Mater. Res.* **28** (1994) 939
4. M. NIINOMI, *Mater. Sci. Eng. A* **243** (1998) 231
5. J. N. KEARNEY and R. J. LOMAS, *Adv. Tiss. Bank.* **1** (1997) 43
6. H. SEEHERMAN, *J. Bone Joint Surg. [Am].* **83**(Supp 1) (2001) S79
7. Y. LIU, E. B. HUNZIKER, P. LAYROLLE, J. D. de BRUIJN and K. de GROOT, *Tissue Eng.* **10** (2004) 101
8. Y. LIU, K. de GROOT and E. B. HUNZIKER, *Bone* **36** (2005) 745
9. S. FALAIZE, S. RADIN and P. DUCHNYNE, *J. Am. Ceram. Soc.* **82** (1999) 969
10. P. SARAVANAPAVAN, J. R. JONES, R. S. PRYCE and L. L. HENCH, *J. Biomed. Mater. Res. A.* **66** (2003) 110
11. I. D. XYNOS, A. J. EDGAR, L. D. K. BUTTERY, L. L. HENCH and J. M. POLAK, *Biochem. Biophys. Res. Commun.* **276** (2000) 461
12. I. D. XYNOS, A. J. EDGAR, L. D. K. BUTTERY, L. L. HENCH and J. M. POLAK, *J. Biomed. Mater. Res.* **55** (2001) 151
13. S. B. NICOLL, S. RADIN, E. M. SANTOS, R. S. TUAN and P. DUCHEYNE, *Biomaterials.* **18** (1997) 853
14. E. M. SANTOS, S. RADIN and P. DUCHEYNE, *Biomaterials.* **20** (1999) 1695
15. S. RADIN, P. DUCHEYNE, T. KAMPLAIN and B.H. TAN, *J. Biomed. Mater. Res.* **57** (2001) 313
16. R. VIITALA, M. JOKINEN, S. TUUSA, J.B. ROSENHOLM and H. JALONEN, *J. Sol-Gel Sci. Tech.* **36** (2005) 147
17. M. C. AGRAWAL, J. BEST, J. D. HECKMAN and B. D. BOYAN, *Protein Biomater.* **16** (1995) 1255
18. H. M. KIM, F. MIYAJI, T. KOKUBO, S. NISHIGUCHI and T. NAKAMURA, *J. Biomed. Mater. Res.* **45** (1999) 100
19. D. K. EGGERS and J. S. VALENTINE, *Protein Sci.* **10** (2001) 250
20. E. LIPPMAA, M. MAGI, A. SAMOSON, G. ENGELHARDT and A. R.GRIMER, *J. Am. chem. Soc.* **102** (1980) 4889
21. H. K. SONG and S. W. SUH, *J. Mol. Biol.* **275** (1998) 347